

Original paper

Wind Field Retrieval in the Coastal Zone Using X-Band Radar Data at Large Incidence Angles

A. E. Korinenko *, V. V. Malinovsky

Marine Hydrophysical Institute of Russian Academy of Sciences, Sevastopol, Russia

* e-mail: korinenko.alex@yandex.ru

Abstract

The paper aims to develop a geophysical model function that allows retrieval of the wind speed vector from a radar signal scattered from the sea surface. During *in situ* experiments on the stationary oceanographic platform in 2022–2024, a database was created which contained radar information, frequency spectra of sea surface elevations, wind speed and direction, and geometric properties of breaking wave crests in the active phase. An MRS-1011 360-degree marine radar (X-band, 3 cm wavelength) transmitting and receiving horizontally polarized signal at large incidence angles was used in the experiments. For these observation conditions, the main informative parameter that governs the radar cross section is the fraction of the sea surface covered by wind wave breaking crests (whitecap coverage). The role of this parameter is qualitatively confirmed by the fact that the radar power and whitecap coverage have similar wind speed dependencies. It was shown that the radar cross section was proportional to the whitecap coverage with 1.47 as the proportionality coefficient. The intensity of wave breaking also depends on the wave age, which leads to the dependency of the radar cross section on the wave development stage. The influence of the wave age on the radar signal level was confirmed experimentally. It was shown that the level of the wind dependency of the radar signal in the “up-wind” direction increased by a factor of 5 when the wave age increased from 0.1 to 1.2. Based on the *in situ* data and physical grounds of the sea surface radar backscatter formation, we suggest a geophysical model function allowing retrieval of wind speed fields in areas within a radius of about a kilometer. The error in wind speed vector magnitude and direction retrieved from radar data was 1.2 m/s and 30°, respectively, compared to the data obtained by the anemometer.

Keywords: navigation radar stations, radar images, normalized radar cross-section, sea surface, wind speed, in situ measurements, wave age, wave breaking

Acknowledgments: The study was carried out with financial support of the Russian Science Foundation grant no. 24-27-20105, <https://rscf.ru/project/24-27-20105>, and under the Agreement with the Department of Education and Science of Sevastopol no. 85 dated June 19, 2024. The authors thank K. A. Pampey for her assistance in *in situ* data processing

For citation: Korinenko, A.E. and Malinovsky, V.V., 2025. Wind Field Retrieval in the Coastal Zone Using X-Band Radar Data at Large Incidence Angles. *Ecological Safety of Coastal and Shelf Zones of Sea*, (1), pp. 26–41.

© Korinenko A. E., Malinovsky V. V., 2025



This work is licensed under a Creative Commons Attribution-Non Commercial 4.0 International (CC BY-NC 4.0) License

Восстановление полей ветра в прибрежной зоне по радиолокационным данным X-диапазона при больших углах наблюдения морской поверхности

А. Е. Кориненко *, В. В. Малиновский

Морской гидрофизический институт РАН, Севастополь, Россия

* e-mail: korinenko.alex@mhi-ras.ru

Аннотация

Цель статьи – разработать геофизическую модельную функцию, позволяющую по радиолокационному сигналу, отраженному от морской поверхности, восстанавливать модуль и направление скорости ветра. В ходе натурных экспериментов на стационарной океанографической платформе в 2022–2024 гг. была сформирована база данных, содержащая радиолокационную информацию, частотные спектры возвышений морской поверхности, скорость и направление ветра, геометрические размеры обрушений в активной фазе. В эксперименте использовалась радиолокационная станция MRS-1011 (X-диапазон, длина электромагнитной волны 3 см), работающая в круговом обзоре на горизонтальной поляризации передачи/приема сигнала при больших углах наблюдения. Для данных условий наблюдений основным информативным параметром, определяющим эффективную площадь рассеяния, является доля морской поверхности, покрытая обрушениями. Качественным подтверждением этого является совпадение ветровой зависимости радиолокационного сигнала с зависимостью от скорости ветра доли моря, занятой обрушениями. Показано, что зависимость эффективной площади рассеяния от суммарной площади обрушений на единице поверхности является линейной с коэффициентом 1.47. Интенсивность обрушений зависит также от возраста волн, что приводит к изменению эффективной площади рассеяния в зависимости от степени развития волнения. Экспериментально установлено влияние возраста волн на уровень сигнала радиолокатора. Показано, что уровень радиолокационного сигнала в направлении «на ветер» увеличивается в пять раз при изменении возраста волн от 0.1 до 1.2. На основании натурных данных и физических представлений о формировании отраженного от морской поверхности радиолокационного сигнала предложена геофизическая модельная функция, которая позволяет определять поля скорости ветра в акваториях радиусом около километра. Ошибка восстановленных по радиолокационным данным модуля и направления скорости ветра составила соответственно 1.2 м/с и 30° по сравнению с информацией, полученной анемометром.

Ключевые слова: радиолокационные станции, радиолокационные изображения, удельная эффективная площадь рассеяния, морская поверхность, скорость ветра, натурные измерения, возраст волн, обрушения ветровых волн

Благодарности: исследование выполнено за счет гранта Российского научного фонда № 24-27-20105, <https://rscf.ru/project/24-27-20105>, и соглашения с Департаментом образования и науки г. Севастополя № 85 от 19.06.2024 г.

Для цитирования: Кориненко А. Е., Малиновский В. В. Восстановление полей ветра в прибрежной зоне по радиолокационным данным X-диапазона при больших углах наблюдения морской поверхности // Экологическая безопасность прибрежной и шельфовой зон моря. 2025. № 1. С. 26–41. EDN JRCXNU.

Introduction

The most effective means of monitoring the aquatic environment under any meteorological conditions and at any time of day and night are radar systems. Currently, algorithms have been developed that use satellite radar information to determine wind speed and direction, surface wave characteristics, and to study eddies and frontal partitioning (see, for example, [1, 2] and the literature cited in these works). These data processing techniques are based on developed theoretical models of the formation of the radar signal reflected from the sea surface at incidence angles of 15–60° [3].

However, satellite data cannot be used for continuous monitoring of wind speed fields, currents and surface wave characteristics in ports, coastal waters and areas of heavy shipping. Navigation radar stations (RS) installed on offshore platforms, ships or onshore structures are used for real-time and continuous monitoring of the selected area. In order to analyse RS data, methods to recover velocity and direction of surface currents and determining characteristics of surface waves were developed and tested (see, for example, [4–6] and the literature cited in these works).

Wind speed reconstruction from radar images is mainly based on empirical models that establish the relationship between the radar signal intensity and wind speed vector magnitude U . In [7], it was proposed to use a third-order geophysical model function (GMF). At wind speeds of ~ 4 and 22 m/s, the errors in retrieved wind speeds were ~ 0.8 and ~ 0.1 m/s, respectively. To determine the wind speed direction, the radar signal intensity, depending on sea surface observation azimuth φ , is approximated by a harmonic function [8]. The value of the angle at which the maximum radar signal value is observed is taken as wind direction φ_U . To determine U , an empirical model function was proposed in [8], in which the radar signal integrated over all azimuth angles was used. Another way to retrieve wind speed vector from marine navigation radar images is to use neural networks [9].

Unfortunately, many papers describing algorithms for wind field retrieval from coastal or ship RS data do not provide information on the linearity of the characteristics of the radar receiving paths and its calibration dependencies. As a result, it is not possible to convert the signal intensity into normalized radar cross-section (NRCS) σ_0 and make comparisons with data from other sources and theoretical models. The empirical GMFs listed above are not based on physical ideas about the formation of the radio signal reflected from the sea surface at large sensing angles. Various methods of smoothing and filtering of the initial signal are applied, which makes it difficult to use the proposed techniques for other types of radars.

Onshore or shipboard radars operate generally in horizontal polarised transmission/reception mode at sea surface sensing angles of 75–89°. Under such observational conditions, the main contribution to the NRCS formation is made by wave breaking [1, 3, 10–12]. In current models, σ_0 depends on fraction of sea surface q with whitecap coverage. Accordingly, the NRCS changes with wind speed variation should be related to the wind dependency of q . At the same time, q depends on the wave age [13–15], which leads to a change in the level of σ_0 for the same wind but different wave ages.

Taking into account the physical state of the sea surface is particularly important for the retrieval of atmospheric parameters in the coastal waters, where the degree of wave development varies widely depending on the wind direction.

The paper aims to develop a semiempirical model of the wind dependency of the sea surface NRCS in the X-band at horizontal polarization of the signal transmission/reception at large incidence angles over a wide range of wave ages.

Experiment location and equipment

The *in situ* experiment was conducted in August – October 2022–2024 on a stationary oceanographic platform located in Blue Bay near the village of Katsiveli, the Southern Coast of Crimea (Fig. 1, *a*). With its coordinates 44°23'38" N, 33°59'09" E, the stationary oceanographic platform is constructed ~ 480 m from the nearest shore point. The depth at the measurement site is about 30 m.

An MRS-1011 (produced by Micran JSC, city of Tomsk) short-range vision radar with high range resolution ($\Delta l = 0.79$ m) transmitting and receiving horizontally polarized signal. The radar power is not more than 1 W, the width of the radiation pattern in the horizontal plane ($\Delta\varphi$) is 1°, in the vertical plane – 30°. In this radar, a continuous linearly modulated signal is generated at an operating frequency of 9430 MHz (wavelength $\lambda_r = 3.2$ cm) modulated by a periodic sawtooth function with a period of 7 ms. The bandwidth of the sensing signal is 200 MHz relative to the operating frequency. The received reflected signal is subjected to amplification and homodyne processing resulting in a beat signal, the spectrum of which represents the range and radar cross-section σ (RCS) of the target.

The radar was mounted on the oceanographic platform at a height of 15 m above sea level (Fig. 1, *b, c*) and was used during the experiment in the circular view mode with an antenna rotation angular velocity of 2.79 rad/s. Due to the radar specific location on the platform, the sea surface viewing sector ranged from 55° to 315° geographic azimuth.

As an example, the inset of Fig. 1, *a* shows a radar image of the sea surface, with clearly visible surface waves. The bright area in the upper left part is due to reflections of the radar signal from the shore. The dark area is the result of shading by the platform elements, in this sector the RS transmitter was not activated.

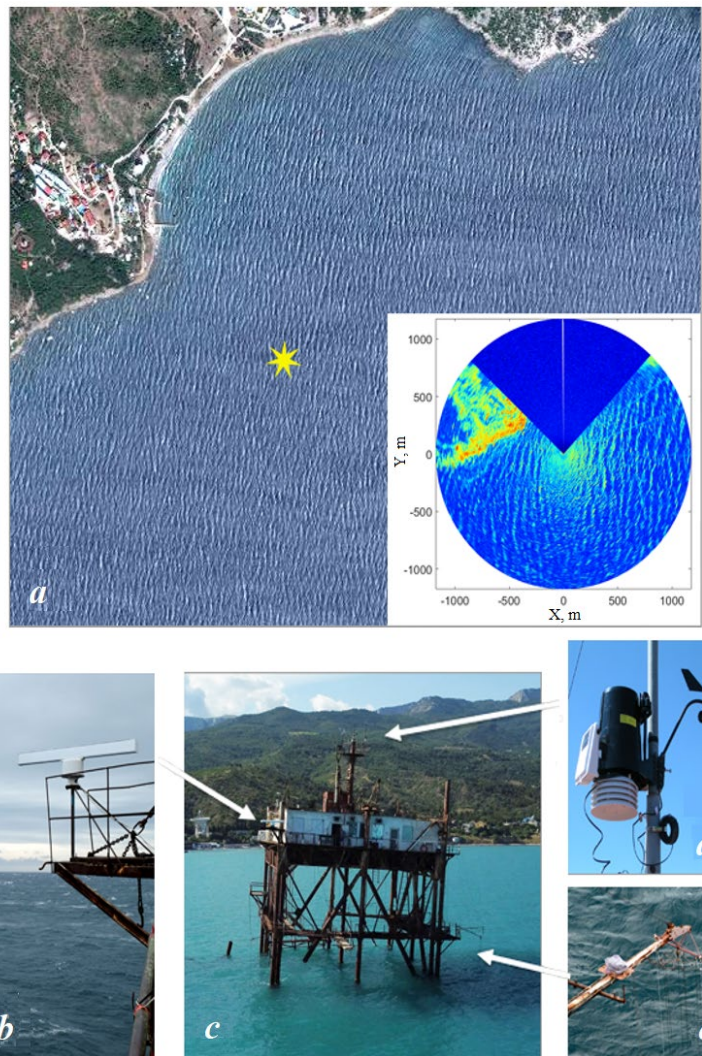


Fig. 1. Study area (a) and equipment used. The star indicates the location of the stationary oceanographic platform; the inset shows a radar image of the sea surface; b – MRS-1011 radar station; c – stationary oceanographic platform, the arrows indicate the location of the equipment shown in b, d, e; d – meteorological station; e – string wave recorder

Wind speed and direction, atmospheric pressure, air temperature and humidity were recorded using a Davis Vantage Pro2 6152 meteorological station located 23 m above sea level on the mast of the oceanographic platform (Fig. 1, d). Water temperature was measured at a depth of 3 m.

Wind speed at 10 m horizon for neutral stratification of the atmospheric boundary layer was calculated using meteorological and surface water temperature data with the COARE 3.0 methodology from [16].

Surface wave characteristics were recorded using a string wave recorder (Fig. 1, *e*). Frequency spectra of sea surface elevations $S(f)$ were obtained as a result of wave data processing. As a rule, during our measurements, in addition to wind waves, ripple waves were also observed. Approach [17] was used to divide the wave frequency spectrum into ripple waves and wind-generated waves. As a result, the values of spectral peak frequency f_p , wave peak frequency f_{pw} and wave age $\alpha = c_{pw}/U$, where c_{pw} is phase velocity of waves at the wave peak frequency, were determined.

The geometric characteristics of wave breaking were determined from video recordings of the sea surface made with a digital video camera. Additional information on the algorithm and calculation of various breaking parameters is given in [18, 19].

Fig. 2 demonstrates the histograms of values U , φ_U and α measured in the experiment. As can be seen from Fig. 2, *a*, wind speed ranged from 2 to 20 m/s, with the majority of observations being made in the U range of 5 to 15 m/s. During the experiments, winds were predominantly easterly ($\varphi_U = 60\text{--}120^\circ$) and westerly ($\varphi_U = 250^\circ$) (Fig. 2, *b*). The wave age distribution shown in Fig. 2, *c* shows that α varied from 0.1 to 3, with $\sim 96\%$ of the wave age values ranging within 0.1–1.2.

Cases when the sea was dominated by ripples were excluded from further processing. Strong modulations of the radar signal caused by ripples can affect the mean values of σ_0 significantly, but are not studied in the paper.

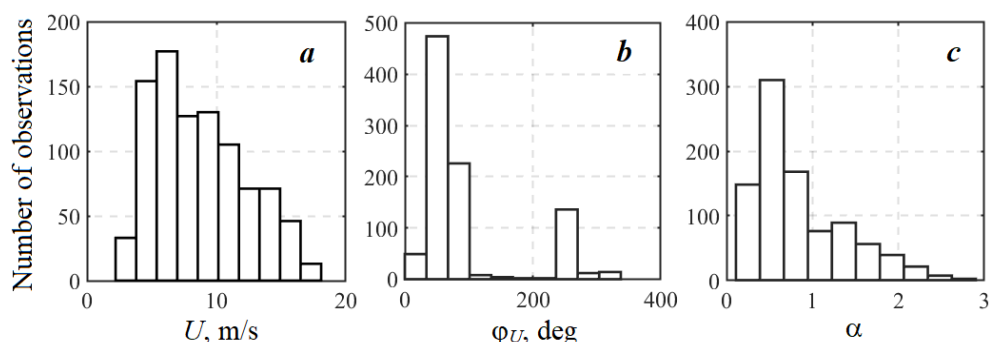


Fig. 2. Histograms of wind and wave measurement conditions: *a* – wind speed; *b* – wind direction; *c* – wave age

Data preprocessing

A radar similar in its technical characteristics to the RS in [20], but with increased transmitter power, was used during the experiments.

To convert conventional units of the radar signal into absolute values of NRCS σ_0 , the RS was calibrated. An inflatable polymer ball (wall thickness ~ 1 mm, diameter $D_{Ball} = 67.5$ cm) with added aluminum powder was used as a target. To give conductive properties, the ball was additionally coated with paint with the addition of aluminum powder. Given that $\lambda_r \ll D_{Ball}/2$, the ball RCS is $\sigma_{Ball} = 0.36$ m². In calm weather, the target was towed by an inflatable boat up to 1000 m from the platform.

Carrying out calibration works is necessary because the obtained values facilitate data interpretation, since the radar scattering models operate with absolute values of the signal. Note that the calibration constants are different for every device.

As was shown in [20], the receiver characteristics of the RS we use are nonlinear. Accordingly, we should expect that the received signal power from the ball P_R will not be described by the basic radar formula. Fig. 3 shows the dependency of P_R/σ_{Ball} value on the distance to the ball R . Measurement data can be described by the following power function

$$P_R / \sigma_{Ball} = C \cdot R^{-d}, \quad (1)$$

where coefficients $C = 1.1 \cdot 10^{12}$ and $d = 3.4$ are obtained by the least squares method.

The magnitude of the reflected signal scattered by the sea depends on the value of irradiated sea surface area S . To exclude this influence, the signal reflected from the sea surface is described as NRCS $\sigma_0 = \sigma / S$, where $S = 2\Delta l R \tan(\Delta\varphi/2)$.

Taking into account the calibration constants, the sea surface NRCS for all points of the radar image was defined as

$$\sigma_0 = C' P R^{2.4},$$

where $C' = 1/[2C \Delta l \tan(\Delta\varphi/2)]$; P is power of the received radar signal.

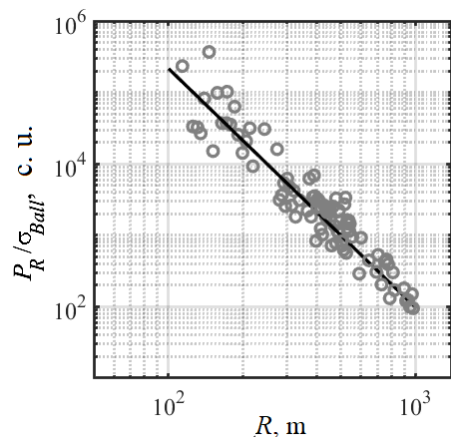


Fig. 3. Dependence of the received signal power normalized to the ball radar cross-section on the distance to the target. The straight line shows approximation by power function (1)

Model of non-Bragg scattering component

A model for the formation of the sea surface radar NRCS is considered in [3]. In general, σ_0 can be represented as the sum of Bragg σ_{0br} and non-Bragg σ_{0nb} scattering components

$$\sigma_0 = \sigma_{0br}(1 - q) + \sigma_{0nb} q.$$

According to [3], σ_{0nb} is formed under conditions of quasi-mirror reflections from very rough parts of the breaking zone, then the whitecap RCS is as follows

$$\sigma_{0nb}(\theta, \varphi) = \sigma_{0wb}(1 + M_{wb} \bar{\theta}_{wb} A_{wb}(\varphi)), \quad (2)$$

$$\sigma_{0nb}(\theta) = (\sec^4(\theta)/s_{wb}^2) \exp(-\tan^2(\theta)/s_{wb}^2) + s_{wb}/s_{wb}^2, \quad (3)$$

where θ is incidence angle from nadir; φ is observation azimuth of the radar station; M_{wb} is modulation transfer function; $\bar{\theta}_{wb}$ – is whitecap average inclination; $A_{wb}(\varphi)$ is coefficient determining the angular distribution of non-Bragg scattering and providing the difference between radar signals in “up-wind” and “down-wind” observations; ε_{wb}^2 is RMS slope of roughness of the breaking zone; ε_{wb} is constant equal to the ratio of the whitecap thickness to its length. At high incidence angles ($\theta > 75^\circ$) [21], the main contribution to the horizontally polarized radar signal is made by σ_{0nb} , and the determining role in expression (3) is played by the second summand, hence, taking into account (2), σ_0 can be written as

$$\sigma_0 = (s_{wb}/s_{wb}^2)(1 + M_{wb} \bar{\theta}_{wb} A_{wb}(\varphi)) q, \quad (4)$$

According to expression (4), σ_0 should not depend on the sea surface observation angle. For very large angles ($\theta > 88-89^\circ$), the NRCS value can be influenced by the effects associated with shading of sea surface areas by long-wave crests. As follows from formula (4), the change in signal power will be determined by the fraction of the sea surface covered by wave breaking.

Traditionally, q is described by power function $q = B_0 U^n$ (see, e. g., [19, 22–24]). However, the large scatter in the data [13, 14] indicates that wind speed by itself does not explain all of the observed variability of q . In particular, according to [13–15], coefficient B_0 is wave age function $B_0 = f(\alpha)$. As function $f(\alpha)$ can be nonlinear, let us define it as power function $f(\alpha) = \alpha^b$. A general form expression for formula (5), which is an analogue of GMF, follows from the above:

$$\sigma_0(\varphi, \theta) = B(\varphi, \theta) \alpha^{b(\varphi, \theta)} U^{n(\varphi, \theta)}, \quad (5)$$

where $b(\varphi, \theta)$, $n(\varphi, \theta)$ and $B(\varphi, \theta)$ are constants.

Note that, since our data were obtained under conditions close to neutral stratification of the atmosphere, we will neglect the manifestation of stratification effects on wave breaking.

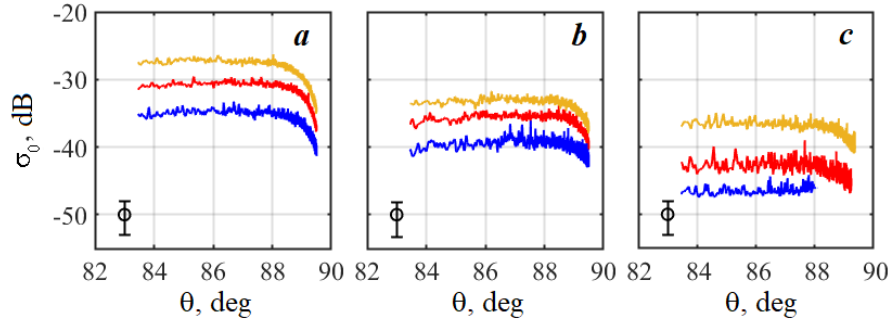


Fig. 4. Normalized radar cross-section (NRCS) of the sea surface as a function of the angle of observation for ‘up-wind’ (a), ‘perpendicular to the wind’ (b) and ‘down-wind’ (c) measurements. The blue line is data averaged over the range $U = 7.0 \pm 1.5$ m/s; the red line is 11.0 ± 1.5 m/s; the orange line is 15.0 ± 1.5 m/s. Confidence intervals are given in the bottom left part of the figure

Analysis of data obtained

Angular dependencies of radar signal

Fig. 4 shows the NRCS dependency on the incidence angle for “up-wind” σ_0^{up} , “perpendicular to the wind” σ_0^{cr} and “down-wind” σ_0^{dw} measurements. The RMS deviation averaged over realisations did not exceed 5 dB. As can be seen from Fig. 4, the sea surface NRCS for incidence angles $83.5 \leq \theta \leq 88^\circ$ is almost unchanged, while at higher values of θ , the NRCS decreases due to the influence of shading by long-wave crests. In order to construct the GMF to recover the wind speed vector, we will consider the mean value of σ_0 over the range of angles (83.5–88°) and on the descending section of σ_0 for values of θ equal to 88 and 89°. For our observational conditions, this corresponds to a distance of 130–860 m.

Wind dependencies of radar signal

Fig. 5 shows an example of wind dependencies σ_0^{up} , σ_0^{cr} , σ_0^{dw} for the range of angles $83.5 \leq \theta \leq 88^\circ$, with the colour of symbols corresponding to the wave age colour scale on the right side.

As follows from Fig. 5, power dependency of σ_0 on wind speed is observed. Note that for the same wind speed at the measurement level, the values of σ_0 increase with increasing α , i. e., in the process of wave development. This regularity is characteristic of all selected observation azimuths. With α changing from 0.1 to 1.2, the weakest growth of σ_0 by ~ 5 times is observed for σ_0^{up} , and the largest NRCS increase by about 30 times is characteristic for σ_0^{cr} . The obtained dependency of σ_0 on wind speed and wave age confirms the appropriateness of describing the sea surface NRCS in form (5).

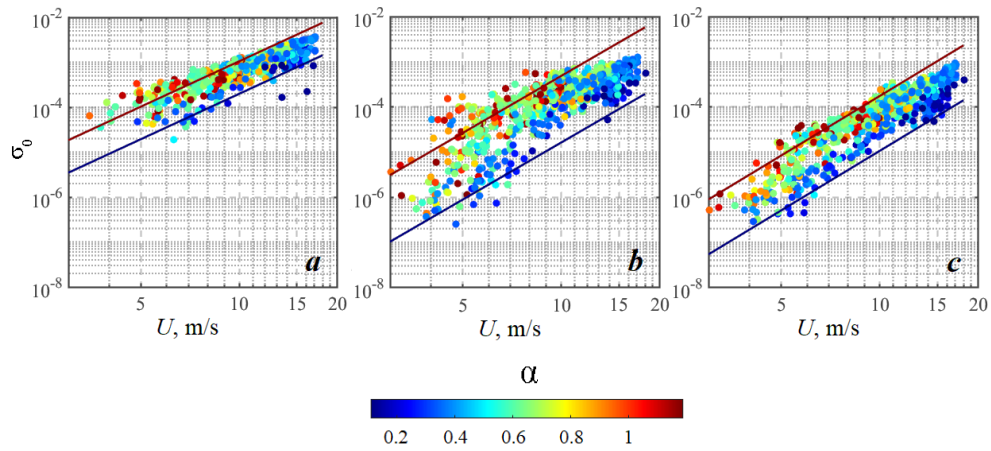


Fig. 5. NRCS of the sea surface as a function of wind speed during ‘up-wind’ (a), ‘perpendicular to the wind’ (b) and ‘down-wind’ (c) sensing. The solid lines correspond to dependence (5) with coefficients given in the table for $\alpha = 0.1$ (lower line) and $\alpha = 1.2$ (upper line)

Coefficients of NRCS wind dependency

| θ | $\varphi = 0^\circ$ | | | $\varphi = 90^\circ$ | | | $\varphi = 180^\circ$ | | |
|----------|---------------------|-----|-----|----------------------|-----|-----|-----------------------|-----|-----|
| | $10^7 B$ | n | b | $10^8 B$ | n | b | $10^8 B$ | n | b |
| 83.5–88 | 4.2 | 3.3 | 0.7 | 2.2 | 4.2 | 1.4 | 0.5 | 4.4 | 1.1 |
| 88.5 | 2.9 | 3.3 | 0.8 | 6.4 | 3.6 | 1.0 | 4.9 | 3.1 | 0.7 |
| 89 | 0.7 | 3.5 | 1.0 | 17.5 | 2.9 | 0.9 | – | – | – |

The values of coefficients B , b , n given in Table for different values of θ and azimuths in the interval $0.1 \leq \alpha \leq 1.2$ were determined by the least squares method from experimental arrays of simultaneous measurements of wind speed, wave age and $\sigma_0(\varphi, \theta)$. In the “up-wind” direction, the values of corresponding powers are almost the same for specified incidence angles θ . The decrease in B level at observation angles $\theta \geq 88.5^\circ$ can be explained by shading conditions.

The obtained values of n fall within the range of wind coefficient estimates known from [14, 25, 26] for the fraction of the sea surface covered by breaking crests.

The NRCS model considered above at large incidence angles (4) indicates that σ_0 is determined by the value of q . Hence, wind dependency σ_0 should be determined by the dependency of q on U . Note that the first two terms in the right-hand side of expression (4) containing s_{wb}^2 , M_{wb} , $\bar{\theta}_{wb}$, can involve in $\sigma_0 = f(U)$, but we did not determine their values. Let us use the archive data of q and the values of σ_0 and q obtained simultaneously during measurements in the experiment.

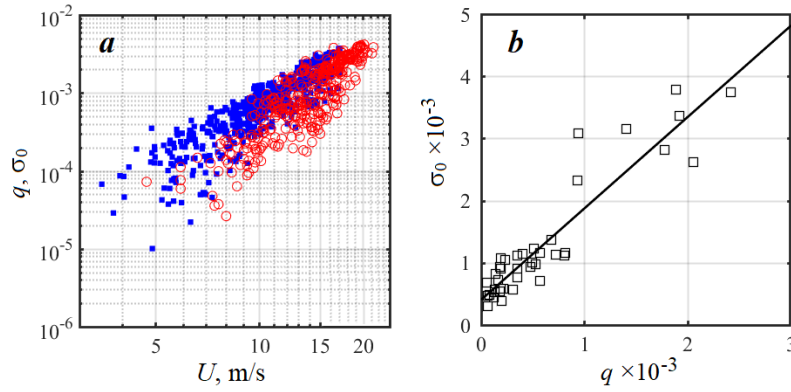


Fig. 6. Fractions of the whitecap coverage and NRCS: *a* – wind dependencies q and σ_0 ; (■ – values of σ_0^{up} at $U = 2.2 \div 17.1$ m/s, ○ – values of q at $U = 4.7 \div 21.4$ m/s) *b* – dependency of NRCS on q derived from synchronous measurements

In Fig. 6, *a*, squares represent the values of σ_0^{up} at wind speeds from 2.2 to 17.1 m/s, circles represent the values of q obtained at $U = 4.7 \div 21.4$ m/s. Both wind dependencies almost coincide, but a slight difference is observed at $U < 10$ m/s; in these cases, a stronger decrease in the value of q is observed with decreasing wind. This can be explained by the fact that during moderate and weak winds, small breaking crests that contribute significantly to the value of q are not identified during video processing [27, 28]. At the same time, such breaking is involved in the formation of the NRCS.

It is of interest to compare σ_0 and the fraction of the surface covered by the active phase of breaking. Indeed, according to model (4), simple relation $\sigma_0 \propto q$ should be observed. Fig. 6, *b* demonstrates the dependency of the NRCS on q obtained from our data as a result of synchronous measurements. As can be seen from Fig. 6, *b*, the dependency of the NRCS on q is satisfactorily described by the linear function shown by the solid line $\sigma_0 = 1.47q$. Such a linear dependency confirms model (4) of the NRCS formation at large incidence angles of the radar signal.

Azimuthal dependencies of radar signal

Previous studies [29–31] have shown that for maritime navigation stations operating on a horizontally polarised signal at $\theta > 75^\circ$, the maximum value of the radar signal is observed in the “up-wind” direction. To describe the azimuthal dependency of the signal and to find the wind speed and direction, we approximate our data by a standard dependency in the form of a restricted Fourier series (see, e. g., [32])

$$\sigma(U, \varphi, \theta) = A_0 + A_1 \cos(\varphi - \varphi_w) + A_2 \cos[2(\varphi - \varphi_w)], \quad (6)$$

where φ_w is direction of azimuthal dependency maximum; A_0, A_1, A_2 are coefficients, which generally depend on U, α, θ and, according to the work ¹⁾, are written as

¹⁾ Ulaby, F.T., Moore, R.K. and Fung, A.K., 1986. *Microwave Remote Sensing: Active and Passive*. Vol. 3. Dedham, MA, USA: Artech House, 2126 p.

$$A_0 = (\sigma_0^{up} + \sigma_0^{cr} + \sigma_0^{dw})/4, \quad (7)$$

$$A_1 = (\sigma_0^{up} - \sigma_0^{dw})/2, \quad (8)$$

$$A_2 = (\sigma_0^{up} - 2\sigma_0^{cr} + \sigma_0^{dw})/4, \quad (9)$$

In our notations, direction $\varphi = \varphi_w$ corresponds to the “up-wind” measurements, $\varphi = \varphi_w + \pi$ – to the “down-wind” ones. In formulas (7)–(9), σ_0^{up} , σ_0^{cr} , σ_0^{dw} are described by expression (6), with the values of coefficients B , b , n given in Table. Fig. 7 shows the NRCS azimuthal dependencies for easterly and westerly wind directions. The line is for dependency (6) considering expressions (5) and (7)–(9). The unknowns in formula (6) are U_{RL} and φ_w , which were determined by the least squares method (with $U_{RL} = 10$ m/s, $\varphi_w = 80^\circ$ for the line in Fig. 7, *a* and with $U_{RL} = 14$ m/s, $\varphi_w = 250^\circ$ for the line in Fig. 7, *b*). The wave age in the radar measurements was calculated from the wind wave elevation spectra.

At moderate wind speeds (Fig. 7, *a*), azimuthal dependency $\sigma_0(\varphi)$ has one pronounced maximum when measuring “up-wind”, with the minimum value observed “down-wind”. When the wind speed increases (Fig. 7, *b*), the azimuthal dependency acquires a bimodal character, a second local maximum appears in the “up-wind” direction. The peculiarities of azimuthal dependencies at large sea surface observation angles are discussed in more detail in [20].

Speeds U_{RL} and φ_w were calculated for the whole data array by the least squares method according to formula (6) using *in situ* radar measurements. Fig. 8 shows the comparison of wind speed direction and vector magnitude retrieved from radar data with those retrieved from the anemometer.

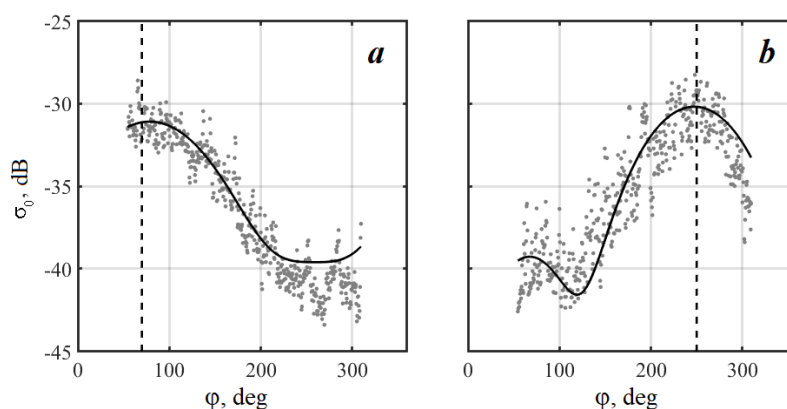


Fig. 7. The sea surface NRCS as an azimuth angle function at $U = 9$ m/s, $\varphi_U = 70^\circ$, $\alpha = 0.8$ (*a*); $U = 15$ m/s, $\varphi_U = 250^\circ$, $\alpha = 0.2$ (*b*). The dashed lines are for wind direction retrieved from the anemometer data

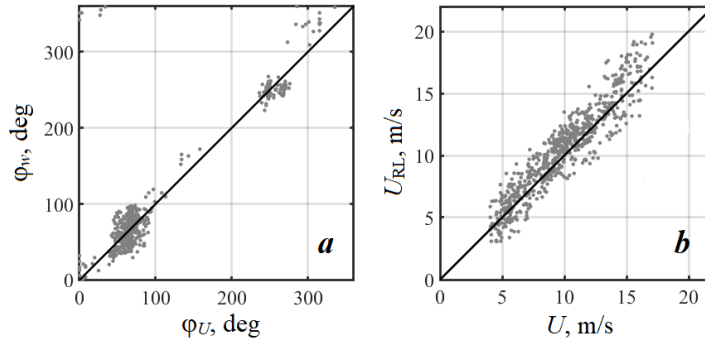


Fig. 8. Wind speed direction (a) and vector magnitude (b) retrieved from the anemometer and radar data. The straight line corresponds to equal values of the two quantities

Fig. 8 shows a linear relationship between φ_w and φ_U as well as between U_{RL} and U , with standard deviations between these pairs of values being 30° and 1.2 m/s, respectively.

Conclusions

The semiempirical model of the wind dependency of the sea surface NRCS is proposed, which makes it possible to retrieve the driving wind speed for X-band radar sensing of the sea surface at large incidence angles. Radar, meteorological, waveform data and video recordings of the sea surface obtained during 2022-2024 at a stationary oceanographic platform in Blue Bay, the Southern Coast of Crimea, were used for the analysis. Measurements were carried out at wind speeds from 4 to 17 m/s. The observed wave age varied from 0.1 to 3, with 96% of the values of α being in the interval $0.1 \leq \alpha \leq 1.2$.

For radar sensing of the sea at large incidence angles, fraction of the sea surface q covered by breaking crests is the main informative parameter that governs NRCS σ_0 . Dependency of the fraction of sea surface covered by breaking crests on wind speed and wave age α results in the corresponding dependencies of σ_0 on wind speed vector magnitude U and wave age.

The contribution of wave breaking to the sea surface NRCS was confirmed experimentally. The linear dependency of σ_0 on the fraction of the sea surface covered by breaking was obtained: $\sigma_0 = 1.47q$. Presented wind dependencies σ_0^{up} and q obtained *in situ*, are almost identical. This result confirms experimentally adopted model $\sigma_0(U) \propto q(U)$ and the essential role of wave breaking in the formation of the radar signal scattered by the sea surface at large incidence angles. It is shown that the degree of wave development affects the NRCS level, which increases five times with increasing wave age from 0.1 to 1.2 for the same “up-wind” direction.

The geophysical model function that takes into account wind speed and wave age α was constructed. Using the results obtained within the geophysical model function, wind speed and wind direction can be retrieved from the radar data. The wind speed vector magnitude and direction calculated from σ_0 coincided satisfactorily with the anemometer readings. The RMS errors of retrieved values U_{RL} and φ_w were 1.2 m/s and 30°, respectively.

REFERENCES

1. Johannessen, J.A., Kudryavtsev, V., Akimov, D., Eldevik, T., Winther, N. and Chapron, B., 2005. On Radar Imaging of Current Features: 2. Mesoscale Eddy and Current Front Detection. *Journal of Geophysical Research*, 110(C7), C07017. <https://doi.org/10.1029/2004JC002802ee>
2. Kudryavtsev, V.N., Chapron, B., Myasoedov, A.G., Collard, F. and Johannessen, J.A., 2013. On Dual Co-Polarized SAR Measurements of the Ocean Surface. *IEEE Geoscience and Remote Sensing letters*, 10(4), pp. 761–765. <https://doi.org/10.1109/LGRS.2012.2222341>
3. Kudryavtsev, V., Hauser, D., Caudal, G. and Chapron, B., 2003. A Semiempirical Model of the Normalized Radar Cross-Section of the Sea Surface. 1. Background Model. *Journal of Geophysical Research: Oceans*, 108(C3), 8054. <https://doi.org/10.1029/2001JC001003>
4. Ivonin, D.V., Telegin, V.A. Bakhanov, V.V. Ermoshkin, A.V. and Azarov, A.I., 2011. Sample Application of a Low-Cost X-Band Monitoring System of Surface Currents at the Black Sea Shore. *Russian Journal of Earth Sciences*, 12(2), pp. 1–8. ES2003. <https://doi.org/10.2205/2011ES000507>
5. Ermoshkin, A.V. and Kapustin, I.A., 2019. Estimation of the Wind-Driven Wave Spectrum Using a High Spatial Resolution Coherent Radar. *Russian Journal of Earth Sciences*, 19(3), ES1005. <https://doi.org/10.2205/2019ES000662>
6. Ermoshkin, A.V., Kapustin, L.A., Molkov, A.A. and Bogatov, N.A., 2020. Determination of the Sea Surface Current by a Doppler X-Band Radar. *Fundamental and Applied Hydrophysics*, 13(3), pp. 93–103. <https://doi.org/10.7868/S2073667320030089> (in Russian).
7. Vicen-Bueno, R., Horstmann, J., Terril, E., de Paolo, T. and Dannenberg, J., 2013. Real-Time Ocean Wind Vector Retrieval from Marine Radar Image Sequences Acquired at Grazing Angle. *Journal of Atmospheric and Oceanic Technology*, 30(1), pp. 127–139. <https://doi.org/10.1175/JTECH-D-12-00027.1>
8. Lund, B., Graber, H. C. and Romeiser, R., 2012. Wind Retrieval from Shipborne Nautical X-Band Radar Data. *IEEE Transactions on Geoscience and Remote Sensing*, 50(10), pp. 3800–3811. <https://doi.org/10.1109/TGRS.2012.2186457>
9. Dankert, H., Horstmann, J. and Rosenthal, W., 2003. Ocean Wind fields retrieved from radar-image sequences. *Journal of Geophysical Research*, 108(C11), 3352. <https://doi.org/10.1029/2003JC002056>
10. Malinovsky, V.V., 1992. Evaluation of the Relationship between Parameters of the Radar Signal Backscattered by the Sea Surface at Grazing Angles and the Wind Wave Breaking Characteristics. *Soviet Journal of Physical Oceanography*, 3(6), pp. 443–454. <https://doi.org/10.1007/BF02197559>
11. Hwang, P.A., Sletten, M.A. and Toporkov, J.V., 2008. Breaking Wave Contribution to Low Grazing Angle Radar Backscatter from the Ocean Surface. *Journal of Geophysical Research: Oceans*, 113(C9), C09017. <https://doi.org/10.1029/2008JC004752>
12. Ermoshkin, A.V., Bakhanov, V.V. and Bogatov, N.A., 2015. Development of an Empirical Model for Radar Backscattering Cross Section of the Ocean Surface at Grazing Angles. *Sovremennye Problemy Distantionnogo Zondirovaniya Zemli iz Kosmosa*, 12(4), pp. 51–59 (in Russian).

13. Zhao, D. and Toba, Y., 2001. Dependence of Whitecap Coverage on Wind and Wind-Wave Properties. *Journal of Oceanography*, 57, pp. 603–615. <https://doi.org/10.1023/A:1021215904955>
14. Brumer, S.E., Zappa, C.J. Brooks, I.M., Tamura, H., Brown, S.M., Blomquist, B.W., Fairall, C.W. and Cifuentes-Lorenzen, A., 2017. Whitecap Coverage Dependence on Wind and Wave Statistics as Observed During SO GasEx and HiWinGS. *Journal of Physical Oceanography*, 47(9), pp. 2211–2235. <https://doi.org/10.1175/JPO-D-17-0005.1>
15. Dulov, V.A., Skiba, E.V. and Kubryakov, A.A., 2023. Landsat-8 Observations of Foam Coverage under Fetch-Limited Wave Development. *Remote Sensing*, 15(9), 2222. <https://doi.org/10.3390/rs15092222>
16. Fairall, C.W., Bradley, E.F., Hare, J.E., Grachev, A.A. and Edson, J.B., 2003. Bulk Parameterization of Air-Sea Fluxes: Updates and Verification for the COARE Algorithm / C. W. Fairall [et al.] // *Journal of Climate*. 16(4), pp. 571–591. [https://doi.org/10.1175/1520-0442\(2003\)016<0571:BPOASF>2.0.CO;2](https://doi.org/10.1175/1520-0442(2003)016<0571:BPOASF>2.0.CO;2)
17. Hanson, J.L. and Phillips, O.M., 1999. Wind Sea Growth and Dissipation in the Open Ocean. *Journal of Physical Oceanography*, 29(8), pp. 1633–1648. [https://doi.org/10.1175/1520-0485\(1999\)029<1633:WSGADI>2.0.CO;2](https://doi.org/10.1175/1520-0485(1999)029<1633:WSGADI>2.0.CO;2)
18. Mironov, A.S. and Dulov, V.A., 2008. Detection of Wave Breaking Using Sea Surface Video Records. *Measurement Science and Technology*, 19(1), 015405. <https://doi.org/10.1088/0957-0233/19/1/015405>
19. Korinenko, A.E., Malinovsky, V.V., Kudryavtsev, V.N. and Dulov, V.A., 2020. Statistical Characteristics of Wave Breakings and their Relation with the Wind Waves' Energy Dissipation Based on the Field Measurements. *Physical Oceanography*, 27(5), pp. 472–488. <https://doi.org/10.22449/1573-160X-2020-5-472-488>
20. Malinovsky, V.V., Korinenko, A.E. and Kudryavtsev, V.N., 2018. Empirical Model of Radar Scattering in the 3-cm Wavelength Range on the Sea at Wide Incidence Angles. *Radiophysics and Quantum Electronics*, 61(2), pp. 98–108. <https://doi.org/10.1007/s11141-018-9874-7>
21. Kudryavtsev, V., Akimov, D., Johannessen, J. and Chapron, B., 2005. On Radar Imaging of Current Features: 1. Model and Comparison with Observations. *Journal of Geophysical Research*, 110(C7), C07016. <https://doi.org/10.1029/2004JC002505>
22. Phillips, O.M., 1988. Radar Returns from the Sea Surface – Bragg Scattering and Breaking Waves. *Journal of Physical Oceanography*, 18(8), pp. 1065–1074. [https://doi.org/10.1175/1520-0485\(1988\)018<1065:RRFTSS>2.0.CO;2](https://doi.org/10.1175/1520-0485(1988)018<1065:RRFTSS>2.0.CO;2)
23. Monahan, E.C. and Woolf, D.K., 1989. Comments on “Variations of Whitecap Coverage with Wind Stress and Water Temperature”. *Journal of Physical Oceanography*, 19(5), pp. 706–709. [https://doi.org/10.1175/1520-0485\(1989\)019<0706:COOWCW>2.0.CO;2](https://doi.org/10.1175/1520-0485(1989)019<0706:COOWCW>2.0.CO;2)
24. Kleiss, J.M. and Melville, W.K., 2010. Observations of Wave Breaking Kinematics in Fetch-Limited Seas. *Journal of Physical Oceanography*, 40(12), pp. 2575–2604. <https://doi.org/10.1175/2010JPO4383.1>
25. Bortkovskii, R.S. and Novak, V.A., 1993. Statistical Dependencies of Sea State on Water Temperature and Wind-Wave Age. *Journal of Marine Systems*, 4(2–3), pp. 161–169. [https://doi.org/10.1016/0924-7963\(93\)90006-8](https://doi.org/10.1016/0924-7963(93)90006-8)
26. Anguelova, M.D. and Webster, F., 2006. Whitecap Coverage from Satellite Measurements: A First Step Toward Modeling the Variability of Oceanic Whitecaps. *Journal of Geophysical Research: Oceans*, 111(C3), C03017. <https://doi.org/10.1029/2005JC003158>
27. Sutherland, P. and Melville, W.K., 2013. Field Measurements and Scaling of Ocean Surface Wave-Breaking Statistics. *Geophysical Research Letters*, 40(12), pp. 3074–3079. <https://doi.org/10.1002/grl.50584>

28. Korinenko, A.E., Malinovsky, V.V. and Kudryavtsev, V.N., 2018. Experimental Research of Statistical Characteristics of Wind Wave Breaking. *Physical Oceanography*, 25(6), pp. 489–500. <https://doi.org/10.22449/1573-160X-2018-6-489-500>
29. Trizna, D.B. and Carlson, D.J., 1996. Studies of Dual Polarized Low Grazing Angle Radar Sea Scatter in Nearshore Regions. *IEEE Transactions on Geoscience and Remote Sensing*, 34(3), pp. 747–757. <https://doi.org/10.1109/36.499754>
30. Hatten, H., Seemann, J., Horstmann, J. and Ziemer, F., 1998. Azimuthal Dependence of the Radar Cross Section and the Spectral Background Noise of a Nautical Radar at Grazing Incidence. In: T. I. Stein, ed., 1998. *Proceedings of IGARSS. Sensing and Managing the Environment. IEEE International Geoscience and Remote Sensing Symposium. Seattle, WA, USA. 6–10 July*. IEEE Publications. Vol. 5, pp. 2490–2492. <https://doi.org/10.1109/IGARSS.1998.702255>
31. Plant, W.J., Keller, W.C., Hayes, K. and Chatham, G., 2010. Normalized Radar Cross Section of the Sea for Backscatter: 1. Mean Levels. *Journal of Geophysical Research: Oceans*, 115(C9), C09032. <https://doi.org/10.1029/2009JC006078>
32. Wentz, F.J., Peteherych, S. and Thomas, L.A., 1984. A Model Function for Ocean Radar Cross Section at 14.6 GHz. *Journal of Geophysical Research: Oceans*, 89(C3), pp. 3689–3704. <https://doi.org/10.1029/JC089iC03p03689>

Submitted 11.07.2024; accepted after review 22.10.2024;
revised 17.12.2024; published 31.03.2025

About the authors:

Aleksandr E. Korinenko, Senior Research Associate, Marine Hydrophysical Institute of RAS (2 Kapitanskaya St., Sevastopol, 299011, Russian Federation), PhD (Phys.-Math.), **Scopus Author ID: 23492523000**, **ORCID ID: 0000-0001-7452-8703**, korinenko.alex@mhi-ras.ru
Vladimir V. Malinovsky, Senior Research Associate, Marine Hydrophysical Institute of RAS (2 Kapitanskaya St., Sevastopol, 299011, Russian Federation), PhD (Phys.-Math.), **ORCID ID: 0000-0002-5799-454X**, **ResearcherID: F-8709-2014**, **Scopus Author ID: 23012976200**, vladimir.malinovsky@mhi-ras.ru

Contribution of the authors:

Aleksandr E. Korinenko – development of techniques and carrying out the experimental studies, paper materials discussion, analysis and summary of the study results, preparation of the paper text

Vladimir V. Malinovsky – development of experimental study techniques, analysis and summary of the study results, preparation of the paper text

All the authors have read and approved the final manuscript.